

Bayesian Optimization of Electrochemical Devices for Electrons-to-Molecules Conversions: The Case of Pulsed CO₂ Electroreduction

Daniel Frey^a, K.C. Neyerlin^{b,}, and Miguel A. Modestino^{a,*}*

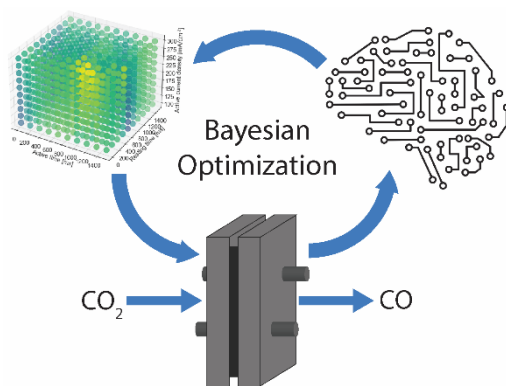
^a Department of Chemical and Biomolecular Engineering, New York University Tandon School of Engineering, Brooklyn, NY 11201, USA

^b Chemistry and Nanoscience Center, National Renewable Energy Laboratory, Golden, CO, 80401, USA

Corresponding Author

* Correspondence to: kenneth.neyerlin@nrel.gov, modestino@nyu.edu

Electrons-to-molecules conversions have emerged as a route to integrate renewable electricity into chemical production processes and ultimately contribute to the decarbonization of chemistry. The practical implementation of these conversions will depend on the optimization of many electrolyzer design and operating parameters. Bayesian optimization (BO) has been shown to be a robust and efficient method for these types of optimization problems where data may be scarce. Here, we demonstrate the use of BO to improve a membrane electrode assembly (MEA) CO₂ electrolyzer, targeting the production of CO through dynamic operation. In a system with intentionally unoptimized components, we first demonstrate the effectiveness of dynamic voltage pulses on CO Faradaic efficiency (FE), then utilize BO for 3D and 4D optimization of pulse times and current densities to achieve a CO partial current density of 189 mA cm⁻². The methodology showcased here lays the groundwork for the optimization of other complex electrons-to-molecules conversions that will be required for the electrification of chemical manufacturing.



High-performing electrochemical reactors could enable electrification and subsequent decarbonization of the chemical industry,¹⁻⁴ a sector responsible for 7% of the global greenhouse gas (GHG) emissions and 10% of the world's energy, primarily in the form of heat derived from fossil-fuel-combustion.^{5, 6} Deploying electrochemical processes to replace current thermochemical routes of chemical production relies on the development of continuous reactors that operate at high-throughput, selectivity, energy conversion efficiency, and leverage low-cost chemical feedstocks. To accelerate the development of such reactors, rapid optimization approaches are needed to identify conditions of operation that maximize their performance. Optimizing these types of reactors is challenging because of the large number of design (*e.g.*, electrocatalyst compositions, device geometries, membrane chemistry) and operating parameters (*e.g.*, temperatures, potentials, flowrates, pressure and their dynamic modulation), which often results in an intractable experimental design space. A promising data-driven optimization strategy to identify global optima with the minimum amount of experimental input is Bayesian Optimization (BO).⁷⁻

¹⁴ BO methods for reactor optimization rely on a surrogate model to statistically predict the mean and uncertainty of a desired performance metric for any possible combination of operating parameters. These surrogate models are then used to decide what experiments will provide the most information from the reactors and allow the identification of the optimum conditions with the minimum number of experiments.¹⁵ Many areas of the chemical sciences have started to use BO to accelerate optimization campaigns, including applications in materials discovery,¹⁶⁻²⁶ design of chemical reactions,²⁷⁻³⁷ and device optimization.³⁸⁻⁴¹ In this study, we demonstrate a general methodology to optimize the operation of electrochemical conversion devices for chemical manufacturing, using dynamic CO₂ electroreduction to CO as a model reaction. This model reaction was chosen (i) because its optimization may lead to a path to upconvert CO₂ into useful

products and possibly reduce carbon emissions,⁴²⁻⁴⁷ (ii) because stable and efficient silver (Ag) electrocatalysts have been widely studied,⁴⁸⁻⁶¹ and (iii) because learnings from this reaction can be translated to the optimization methodology of other emerging electrochemical conversion processes of relevance to chemical manufacturing (e.g., ethylene or propylene production and functionalization).⁶²⁻⁶⁸

To demonstrate the effectiveness of BO in optimizing CO₂ electroreduction, we developed a methodology to maximize CO production under dynamic potential pulsing with current densities and pulse times as optimization parameters. Pulsed potentials, and resultingly current density, can elicit favorable transient behavior, affecting hydrodynamics, the electrocatalyst double layer, reactant concentration, and the presence or absence of different intermediates and adsorbates on the electrode surface microenvironment.⁶⁹⁻⁷¹ More specifically, previous studies have shown that the use of dynamic voltage pulses can control selectivity and/or stability of CO₂ electroreduction.^{56, 72-84} All of these studies used a systematic approach to determine optimal operation conditions leading to large information gaps between the tested experimental conditions and possibly sub-optimal parameter selection. In this study, we leverage these previous findings to demonstrate the use of BO to rapidly optimize the dynamic operating conditions in industrially relevant zero-gap electrochemical conversion devices. Our findings demonstrate the ability to map performance metrics in large design spaces with high accuracy while also identifying optimal operation strategies with a low number of experiments.

To understand the baseline performance of the reactor, constant current experiments were performed to characterize the CO Faradaic efficiency (FE_{CO}). Figure 1A shows that the FE_{CO} increases with current density until 200 mA cm⁻², and then decreases as the current density increases to 500 mA cm⁻². This trend is consistent with observations from other studies on CO

production on silver electrodes.^{48, 51, 52, 57, 59} As an initial comparison of constant current operation versus pulsed operation, six combinations of active pulse time (t_{act}) and resting pulse time (t_{rest}) were tested. For these experiments, the active voltage was set to 3 V and the resting voltage set to 1.1 V, leading to an active total current density of 200-240 mA cm⁻². Our results show that FE_{CO} can be improved when appropriate pulsed potentials are applied [Figure 1(B)], as previously demonstrated in other reactor configurations^{56, 69, 76, 81-83}. These initial results serve as a baseline for determining the optimal combination of active and resting pulse durations using BO.

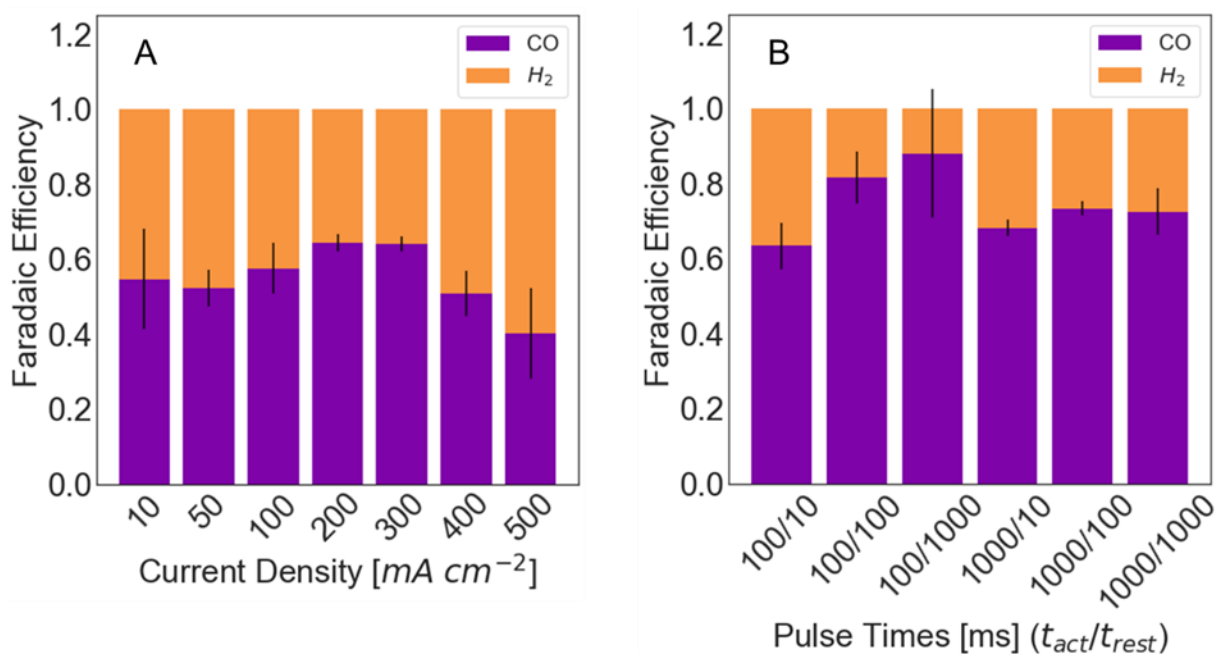


Figure 1. Faradaic efficiency of CO for (A) constant current experiments and (B) pulsed experiments. For the pulsed experiments, the active voltage was set to 3 V and the resting voltage was set to 1.1 V.

In order to gain insights on the effects that active pulse duration and rest pulse duration have on FE_{CO} and production rate, two-dimensional (2D) maps were constructed based on a Gaussian process regressor surrogate model (GPR SM) trained with experimental data. Figure 2 shows scatter plots of FE_{CO} and CO partial current density obtained from 34 experiments where

operating conditions were randomly selected throughout the design space (*i.e.*, Pulse times in the range 10-1500 ms). The background of each plot shows the SM predictions based on the experimental data collected. Figure 2A shows the relationship between the pulse times and FE_{CO} . These results suggest that pulse time combinations with similar t_{act} and t_{rest} have the highest FE_{CO} .

Figure 2B shows that the average CO partial current density (j_{CO}) generally improves as the total active time increases. j_{CO} averages the partial current density over both the active and resting pulse times. This result is likely because longer active times allow for a larger quantity of CO_2 to be reduced, despite the fact that maximum FE_{CO} may be achieved with lower active times. To better understand the effect of the total active time on reactor performance, Figure S1 in the Support information shows FE_{CO} and j_{CO} as a function of the ratio between t_{act} and t_{rest} . As the ratio increases, the j_{CO} increases monotonically, until it reaches a value of 2.5 when it asymptotically starts to approach the limit of j_{CO} at a constant current of 200 mA cm^{-2} . This result suggests the main driver of performance is the amount time the cell is active. However, analyzing CO partial current density during the active time (j_{CO}^{act}) at various pulse time combinations (Figure S2), it is evident that longer rest duration allowed for higher j_{CO}^{act} , possibly due to an increased CO_2 concentration near the electrode. Our results identified conditions with maximum FE_{CO} of 0.79 at $t_{rest} = 170 \text{ ms}$ and $t_{act} = 350 \text{ ms}$, and maximum j_{CO} of 126 mA cm^{-2} at $t_{rest} = 10 \text{ ms}$ and $t_{act} = 830 \text{ ms}$. While FE_{CO} is an important metric for some applications where maintaining maximum energy efficiency is desirable, we decided to focus this study on the optimization of j_{CO} to achieve reactor operations with high throughput.

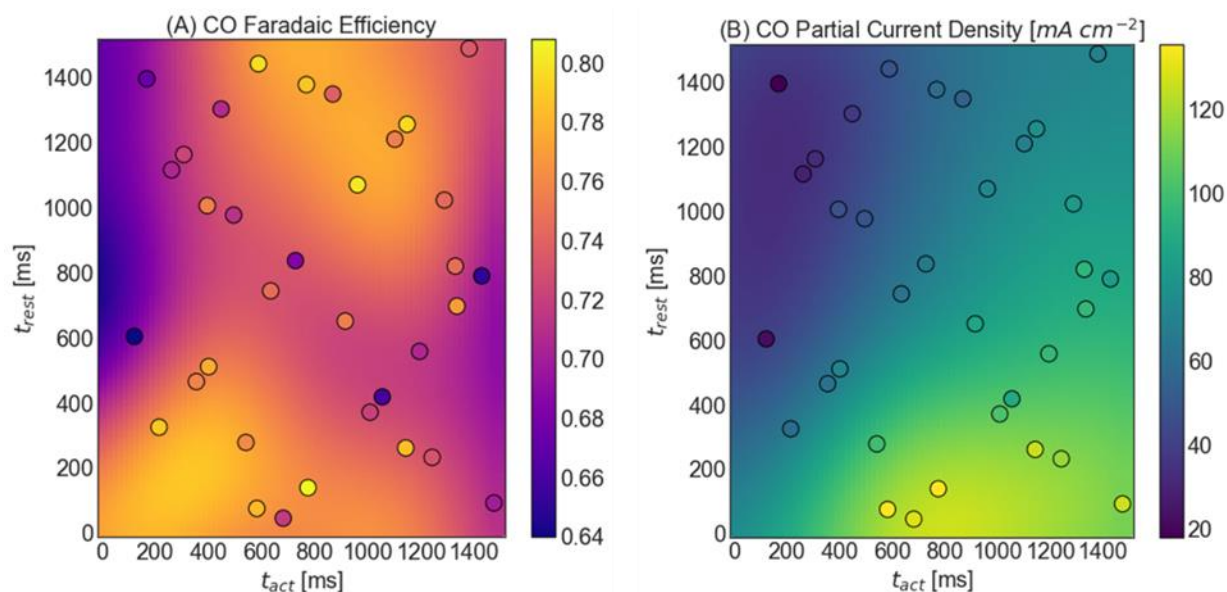


Figure 2. 2D maps of (A) FE_{CO} and (B) CO partial current density while varying t_{act} and t_{rest} .

Experimental conditions are shown with a black outline. The background displays the GPR prediction based on the observed experimental values. Active current density was set to 200 mA cm^{-2} and resting current density was set to 0 mA cm^{-2} .

While results presented above demonstrated the potential to modulate reactor performance by controlling pulse times, to achieve higher production rates it was important to include the current density of active pulses (j_{act}) as an optimization parameter. Given the increase in design space and the resulting requirement for larger data sets, we implemented a BO approach to identify the optimal conditions for maximum j_{CO} . A total of 50 experiments were performed in the optimization campaign in batches of four. Figure 3A shows how the experiments selected by the BO algorithm explored the entire design space initially and focused on parameters with high CO production during later stages of the search. Figure 3B shows j_{CO} during the optimization process. The maximum production rate was found at $t_{rest} = 10 \text{ ms}$, $t_{act} = 435 \text{ ms}$, and $j_{act} = 300 \text{ mA cm}^{-2}$ at

experiment 42, leading to a $j_{CO} = 189 \text{ mA cm}^{-2}$, representing only a small increase from the case where a constant total current density of 300 mA cm^{-2} was applied and $j_{CO} = 180 \text{ mA cm}^{-2}$.

2D slices of predictions from SM trained with data from the 50 experiments performed are shown in Figure 3C-E. The predicted j_{CO} are shown in Figure 3C at $j_{act} = 100$ and 300 mA cm^{-2} . For $j_{act} = 300 \text{ mA cm}^{-2}$, the predicted maximum j_{CO} was at $t_{act} = 545 \text{ ms}$ and $t_{rest} = 48 \text{ ms}$, while for j_{act} of 100 mA cm^{-2} , the optimum j_{CO} was at $t_{act} = 545 \text{ ms}$ and $t_{rest} = 10 \text{ ms}$. As j_{act} increases, the predicted maximum j_{CO} increased from 53.5 to 119 mA cm^{-2} . These results agree with the results from the 2D experiments, in which the t_{act}/t_{rest} ratio and j_{CO} increase together. The FE_{CO} predictions are shown in Figure 3D. At $j_{act} = 100 \text{ mA cm}^{-2}$, the maximum FE_{CO} is predicted to be 0.83 at $t_{act} = 1500 \text{ ms}$ and $t_{rest} = 736 \text{ ms}$. As j_{act} increases, the location in the pulse time design space of the maximum FE_{CO} shifts towards a shorter t_{act} . This results in the predicted maximum FE_{CO} at $j_{act} = 300 \text{ mA cm}^{-2}$ to be 0.84 at $t_{act} = 583 \text{ ms}$ and $t_{rest} = 660 \text{ ms}$. The shift towards shorter t_{act} at higher j_{act} is likely due to the faster depletion of CO_2 which results in the need for lower t_{act} to not deplete the CO_2 concentration at or near the electrocatalyst surface. In order to provide insights into the prediction accuracy of the GPR SM, Figure 3E shows the normalized standard deviation of the predictions throughout the design space. At $j_{act} = 100 \text{ mA cm}^{-2}$, the predictions in a large fraction of the space have near-average standard deviations due to extensive exploration around this j_{act} by the BO algorithm, while at 300 mA cm^{-2} , accurate predictions are mostly concentrated near the optimal conditions due to the large numbers of experiments performed around optimal conditions during the exploitation stage of BO.

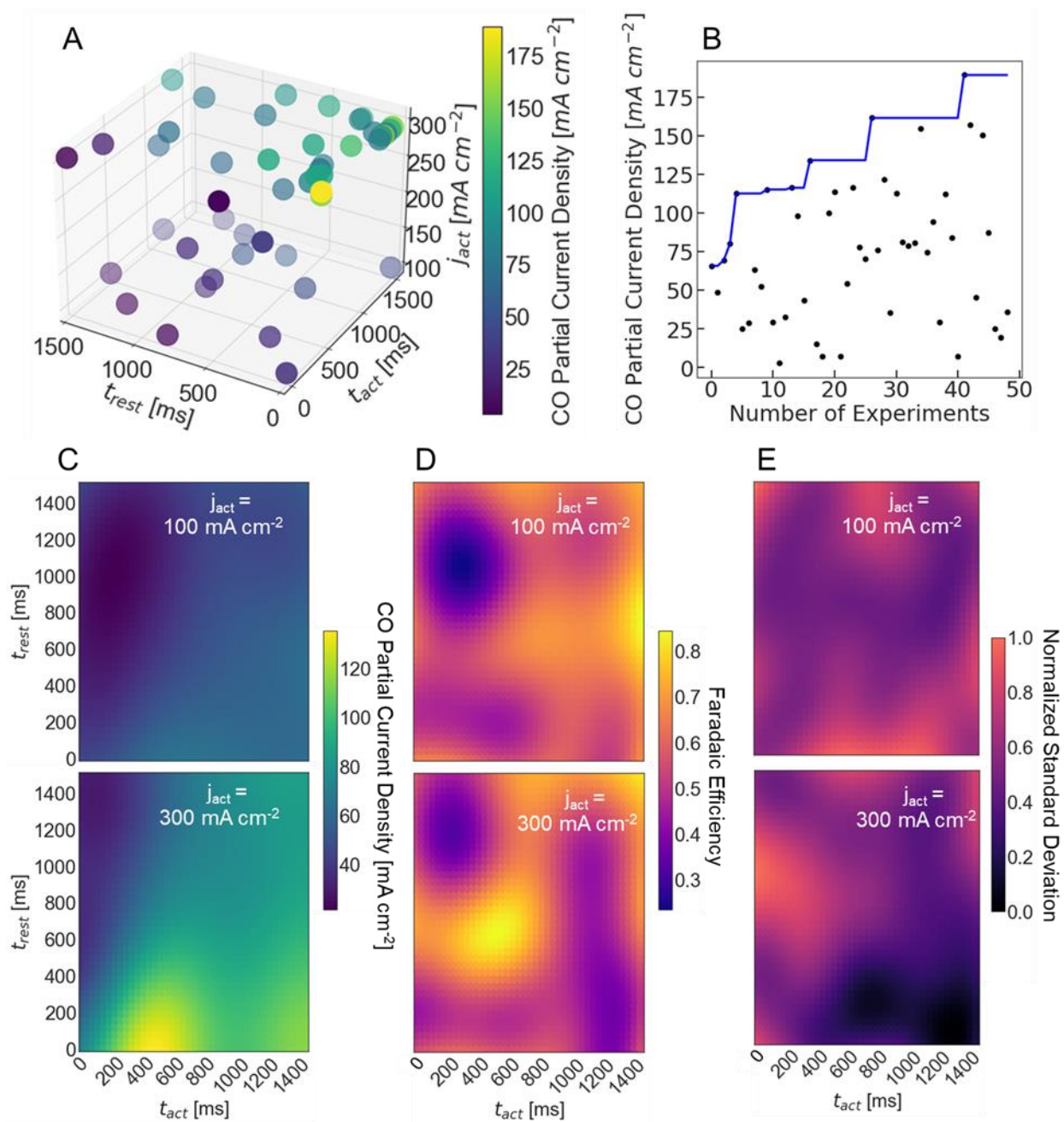


Figure 3. (A) Location in 3D design space of the 50 experimental conditions studied in the optimization campaign, varying j_{act} , t_{act} , and t_{rest} . Color of the marker indicates the CO partial current density at that condition. (B) CO partial current density throughout the optimization campaign. Black markers indicate the experimental points and the blue line indicates the highest value achieved. (C-E) 2D slices at $j_{act} = 100 \text{ mA cm}^{-2}$ and 300 mA cm^{-2} showing the GPR

predictions of (C) CO partial current density, (D) CO_{FE}, and (E) normalized standard deviation, based on the 50 observed experiments. Resting current density was set to 0 mA/cm².

Having identified optimal t_{act} , t_{rest} , and j_{act} with a fixed resting current density, $j_{rest} = 0$ mA cm⁻², the next step in the optimization was to explore possible improvements by modulating j_{rest} . Figure 4A presents the 50 experimental conditions tested in the entire design space, showing a few conditions dispersed in the entire design space that were selected during the exploration stage of BO, and a concentration of experiments near high j_{act} and t_{act} , and low t_{rest} during the exploitation stage when the algorithm seeks to identify the optimal conditions. Figure 4B displays the improvement in j_{CO} as a function of experiments performed and identifies conditions that lead to a CO partial current density of 166 mA cm⁻² after the 50 experiments. It must be noted that this j_{CO} is lower than the one found in the 3D optimization campaign with the same number of experiments. This suggests that the increased dimensionality of the optimization problem requires a larger number of experiments to approach the optimum. Furthermore, our results demonstrate that the impact of j_{rest} is not significant in the performance of the reactor, possibly because optimal t_{rest} values are small and thus any change in j_{rest} would only impact a small fraction of the operation time. These results underscore the need to carefully select optimization parameters so that the tradeoff between potential performance improvements and the need for larger experimental campaigns is balanced.

To gain insights into the effects of the 4 optimization parameters on the CO partial current density, Figure 4C shows the SM predictions of j_{CO} as 2D slices at the optimal location of the other two variables. These results are consistent with those of the 2D and 3D optimizations, where the high j_{CO} values are found at low t_{rest} , and high t_{act} , and j_{act} . 2D slices of the FE_{CO} predictions are shown in Figure 4D. The trends observed for FE_{CO} predictions are different than for j_{CO} , with high

FE_{CO} found at low t_{rest} , t_{act} and j_{act} . Figure 4E shows the standard deviations from the SM predictions of the 2D slices. As observed from the results, the increase in dimensionality results in larger standard deviations for a large fraction of the design space, underscoring the need for large datasets when the number of optimization parameters increase.

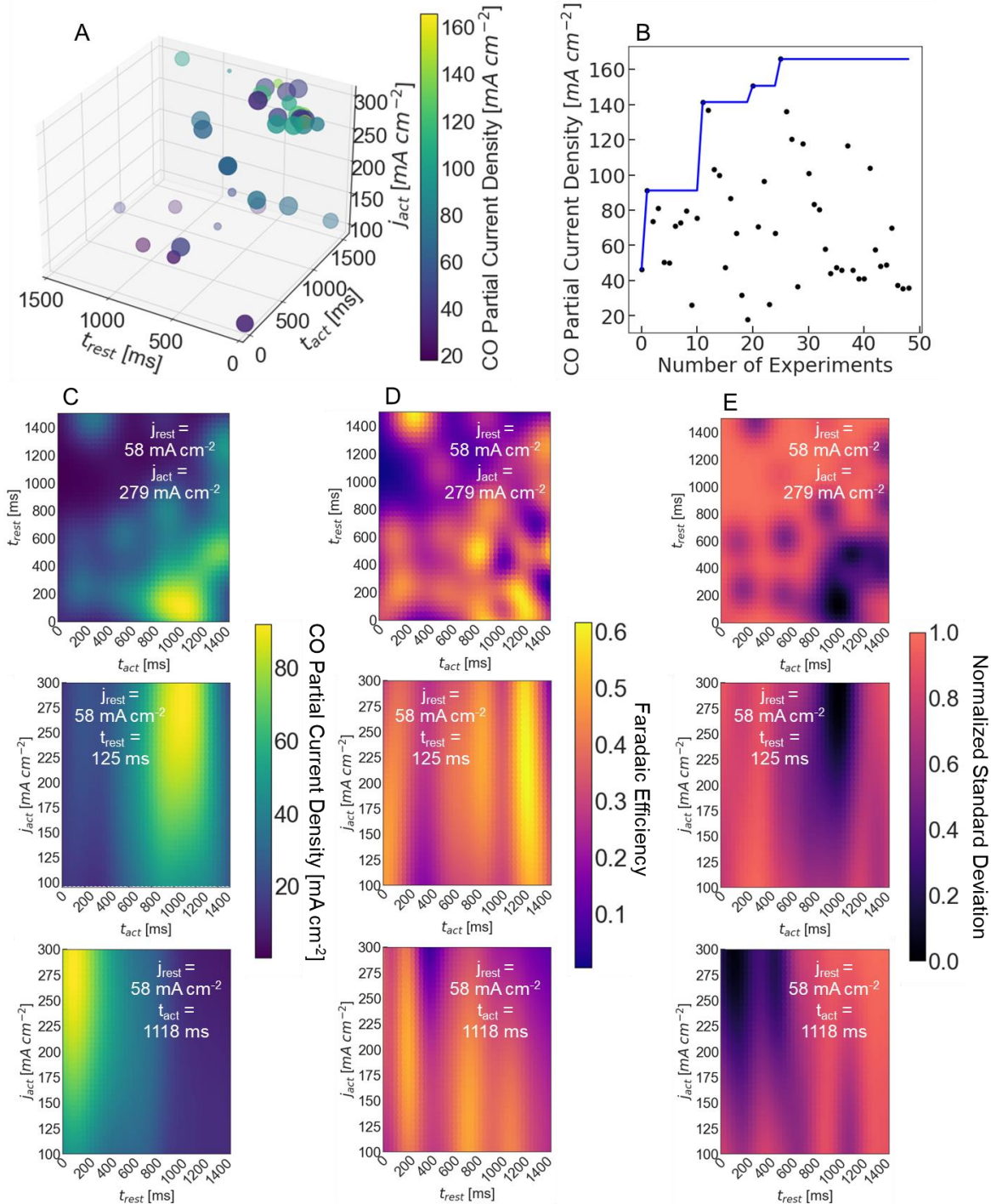


Figure 4. (A) Location in the 4D design space of the 50 experimental conditions studied in the optimization campaign, varying j_{act} , t_{act} , and t_{rest} . Size of the marker indicates the j_{rest} value and the color of the marker indicates the CO partial current density at that condition. (B) CO partial current density throughout the optimization campaign. Black markers indicate the experimental points and the blue line indicates the highest value achieved. (C-E) 2D slices at the optimal locations for CO partial current density of the other two variables, which are shown on the graph. The slices show the GPR predictions of (C) CO partial current density, (D) CO_{FE} , and (E) normalized standard deviation, based on the 50 observed experiments.

The study described above introduces a BO methodology to improve the performance of dynamic electrochemical conversion devices for electrons-to-molecules conversions. This methodology allowed us to identify pulsed operation regimes in a CO_2 electrolyzer with improved selectivity and production rates. 3D optimization of t_{rest} , t_{act} and j_{act} with only 50 experiments showed improvements from $j_{CO} = 115 \text{ mA cm}^{-2}$ in the initial set of 10 experiments, to a maximum of 189 mA cm^{-2} . In the case of 4D optimization of t_{rest} , t_{act} , j_{act} and j_{rest} , the optimization campaign achieved an improvement from $j_{CO} = 91 \text{ mA cm}^{-2}$ in the initial set of 10 experiments, to a maximum of $j_{CO} = 166 \text{ mA cm}^{-2}$. Because of the lower optimum value discovered in the 4D optimization, the 50 experiments in this case were not as effective at searching the design space as the 3D optimization. This result underscores the need for larger datasets at higher dimensions, and the need to carefully select optimization variables or to implement dimensionality reduction approaches (*e.g.*, principal component analysis) to minimize the number of experiments required in high dimensionality space. Furthermore, the statistical GPR surrogate models used in the BO methodology allowed us to develop performance (*i.e.*, j_{CO} or FE_{CO}) maps covering conditions beyond the ones tested. These maps provide further insights into the behavior of electrochemical

devices across the parameter space. While this study focused on implementing a BO methodology for CO₂ electrolyzers as a test case, the framework presented here can be generalized to the optimization of other electrochemical devices for the production of high-value chemicals that require complex reactions and the delicate control of the electrode microenvironment.

ASSOCIATED CONTENT

Supporting Information. Methods and additional figures are provided in the Supporting Information file.

AUTHOR INFORMATION

Corresponding Authors

Miguel A. Modestino – Department of Chemical Engineering, New York University, New York, New York 11201, United States; Email: modestino@nyu.edu

K.C. Neyerlin – Chemistry and Nanoscience Center, National Renewable Energy Laboratory, Golden, CO, 80401, United States; Email: kenneth.neyerlin@nrel.gov

Authors

Daniel Frey - Department of Chemical Engineering, New York University, New York, New York 11201, United States; Email: dmf456@nyu.edu

Notes

MAM is a director and has a financial interest in Sunthetics, Inc., a start-up company in the machine learning optimization space.

ACKNOWLEDGMENT

This work was authored in part by Alliance for Sustainable Energy, LLC, the manager and operator of the National Renewable Energy Laboratory for the U.S. Department of Energy (DOE) under Contract No. DE-AC36-08GO28308. Funding provided by the Office of Science Graduate Student Research program under Contract No. DE-SC0014664. The views expressed in the article do not necessarily represent the views of the DOE or the U.S. Government. The U.S. Government retains and the publisher, by accepting the article for publication, acknowledges that the U.S. Government retains a nonexclusive, paid-up, irrevocable, worldwide license to publish or reproduce the published form of this work, or allow others to do so, for U.S. Government purposes.

REFERENCES

1. Blanco, D. E.; Modestino, M. A., Organic electrosynthesis for sustainable chemical manufacturing. *Trends in Chemistry* **2019**, *1* (1), 8-10.
2. Biddinger, E. J.; Modestino, M. A., Electro-organic syntheses for green chemical manufacturing. *Electrochem. Soc. Interface* **2020**, *29*, 43-47.
3. Schiffer, Z. J.; Limaye, A. M.; Manthiram, K., Thermodynamic Discrimination between Energy Sources for Chemical Reactions. *Joule* **2021**, *5* (1), 135-148.
4. De Luna, P.; Hahn, C.; Higgins, D.; Jaffer, S. A.; Jaramillo, T. F.; Sargent, E. H., What would it take for renewably powered electrosynthesis to displace petrochemical processes? *Science* **2019**, *364* (6438).
5. González-Garay, A.; Mac Dowell, N.; Shah, N., A carbon neutral chemical industry powered by the sun. *Discover Chemical Engineering* **2021**, *1* (1), 1-22.
6. Kätelhön, A.; Meys, R.; Deutz, S.; Suh, S.; Bardow, A., Climate change mitigation potential of carbon capture and utilization in the chemical industry. *Proceedings of the National Academy of Sciences* **2019**, *116* (23), 11187-11194.
7. Xue, D.; Balachandran, P. V.; Hogden, J.; Theiler, J.; Xue, D.; Lookman, T., Accelerated search for materials with targeted properties by adaptive design. *Nat. Commun.* **2016**, *7* (1), 1-9.
8. Vahid, A.; Rana, S.; Gupta, S.; Vellanki, P.; Venkatesh, S.; Dorin, T., New bayesian-optimization-based design of high-strength 7xxx-series alloys from recycled aluminum. *JOM* **2018**, *70* (11), 2704-2709.
9. Li, C.; de Celis Leal, D. R.; Rana, S.; Gupta, S.; Sutti, A.; Greenhill, S.; Slezak, T.; Height, M.; Venkatesh, S., Rapid Bayesian optimisation for synthesis of short polymer fiber materials. *Scientific reports* **2017**, *7* (1), 1-10.
10. Abdelrahman, H.; Berkenkamp, F.; Poland, J.; Krause, A., Bayesian optimization for maximum power point tracking in photovoltaic power plants. *2016 European Control Conference (ECC)* **2016**, 2078-2083.
11. Kikuchi, S.; Oda, H.; Kiyohara, S.; Mizoguchi, T., Bayesian optimization for efficient determination of metal oxide grain boundary structures. *Physica B: Condensed Matter* **2018**, *532*, 24-28.
12. Khajah, M. M.; Roads, B. D.; Lindsey, R. V.; Liu, Y.-E.; Mozer, M. C., Designing engaging games using Bayesian optimization. *Proceedings of the 2016 CHI conference on human factors in computing systems* **2016**, 5571-5582.
13. Lorenz, R.; Violante, I. R.; Monti, R. P.; Montana, G.; Hampshire, A.; Leech, R., Dissociating frontoparietal brain networks with neuroadaptive Bayesian optimization. *Nat. Commun.* **2018**, *9* (1), 1-14.
14. Frey, D.; Shin, J.; Musco, C.; Modestino, M. A., Chemically-informed data-driven optimization (ChIDDO): Leveraging physical models and Bayesian learning to accelerate chemical research. *Reaction Chemistry & Engineering* **2022**.
15. Frazier, P., A tutorial on Bayesian optimization. *arXiv: 1807.02811* **2018**.
16. Herbol, H. C.; Hu, W.; Frazier, P.; Clancy, P.; Poloczek, M., Efficient search of compositional space for hybrid organic-inorganic perovskites via Bayesian optimization. *Computational Materials* **2018**, *4* (1), 1-7.

17. Herbol, H. C.; Poloczek, M.; Clancy, P., Cost-effective materials discovery: Bayesian optimization across multiple information sources. *Materials Horizons* **2020**.
18. Yamashita, T.; Sato, N.; Kino, H.; Miyake, T.; Tsuda, K.; Oguchi, T., Crystal structure prediction accelerated by Bayesian optimization. *Physical Review Materials* **2018**, *2* (1), 013803.
19. Ju, S.; Shiga, T.; Feng, L.; Hou, Z.; Tsuda, K.; Shiomi, J., Designing nanostructures for phonon transport via Bayesian optimization. *Physical Review X* **2017**, *7* (2), 021024.
20. Ueno, T.; Rhone, T. D.; Hou, Z.; Mizoguchi, T.; Tsuda, K., COMBO: an efficient Bayesian optimization library for materials science. *Materials discovery* **2016**, *4*, 18-21.
21. Hashimoto, W.; Tsuji, Y.; Yoshizawa, K., Optimization of Work Function via Bayesian Machine Learning Combined with First-Principles Calculation. *The Journal of Physical Chemistry C* **2020**, *124* (18), 9958-9970.
22. Balachandran, P. V.; Kowalski, B.; Sehirlioglu, A.; Lookman, T., Experimental search for high-temperature ferroelectric perovskites guided by two-step machine learning. *Nat. Commun.* **2018**, *9* (1), 1-9.
23. Higgins, K.; Valleti, S. M.; Ziatdinov, M.; Kalinin, S. V.; Ahmadi, M., Chemical Robotics Enabled Exploration of Stability in Multicomponent Lead Halide Perovskites via Machine Learning. *ACS Energy Lett.* **2020**, *5* (11), 3426-3436.
24. Ling, J.; Hutchinson, M.; Antono, E.; Paradiso, S.; Meredig, B., High-dimensional materials and process optimization using data-driven experimental design with well-calibrated uncertainty estimates. *Integrating Materials and Manufacturing Innovation* **2017**, *6* (3), 207-217.
25. MacLeod, B. P.; Parlane, F. G.; Morrissey, T. D.; Häse, F.; Roch, L. M.; Dettelbach, K. E.; Moreira, R.; Yunker, L. P.; Rooney, M. B.; Deeth, J. R., Self-driving laboratory for accelerated discovery of thin-film materials. *Science Advances* **2020**, *6* (20), eaaz8867.
26. Min, K.; Cho, E., Accelerated discovery of potential ferroelectric perovskite via active learning. *Journal of Materials Chemistry C* **2020**, *8* (23), 7866-7872.
27. Park, S.; Na, J.; Kim, M.; Lee, J. M., Multi-objective Bayesian optimization of chemical reactor design using computational fluid dynamics. *Comput. Chem. Eng.* **2018**, *119*, 25-37.
28. Schweidtmann, A. M.; Clayton, A. D.; Holmes, N.; Bradford, E.; Bourne, R. A.; Lapkin, A. A., Machine learning meets continuous flow chemistry: Automated optimization towards the Pareto front of multiple objectives. *Chem. Eng. J.* **2018**, *352*, 277-282.
29. Burger, B.; Maffettone, P. M.; Gusev, V. V.; Aitchison, C. M.; Bai, Y.; Wang, X.; Li, X.; Alston, B. M.; Li, B.; Clowes, R., A mobile robotic chemist. *Nature* **2020**, *583* (7815), 237-241.
30. Granda, J. M.; Donina, L.; Dragone, V.; Long, D.-L.; Cronin, L., Controlling an organic synthesis robot with machine learning to search for new reactivity. *Nature* **2018**, *559* (7714), 377-381.
31. Guo, Z.; Wu, S.; Ohno, M.; Yoshida, R., Bayesian Algorithm for Retrosynthesis. *Journal of Chemical Information and Modeling* **2020**, *60* (10), 4474-4486.
32. Häse, F.; Roch, L. M.; Aspuru-Guzik, A., Chimera: enabling hierarchy based multi-objective optimization for self-driving laboratories. *Chemical science* **2018**, *9* (39), 7642-7655.
33. Häse, F.; Roch, L. M.; Aspuru-Guzik, A., Next-generation experimentation with self-driving laboratories. *Trends in Chemistry* **2019**, *1* (3), 282-291.
34. Kondo, M.; Wathsala, H.; Sako, M.; Hanatani, Y.; Ishikawa, K.; Hara, S.; Takaai, T.; Washio, T.; Takizawa, S.; Sasai, H., Exploration of flow reaction conditions using machine-learning for enantioselective organocatalyzed Rauhut–Currier and [3+ 2] annulation sequence. *Chem. Commun.* **2020**, *56* (8), 1259-1262.

35. Shields, B. J.; Stevens, J.; Li, J.; Parasram, M.; Damani, F.; Alvarado, J. I. M.; Janey, J. M.; Adams, R. P.; Doyle, A. G., Bayesian reaction optimization as a tool for chemical synthesis. *Nature* **2021**, *590* (7844), 89-96.
36. Reker, D.; Hoyt, E. A.; Bernardes, G. J.; Rodrigues, T., Adaptive Optimization of Chemical Reactions with Minimal Experimental Information. *Cell Reports Physical Science* **2020**, *1* (11), 100247.
37. Kim, K.; Lee, W. H.; Na, J.; Hwang, Y.; Oh, H.-S.; Lee, U., Data-driven pilot optimization for electrochemical CO mass production. *Journal of Materials Chemistry A* **2020**, *8* (33), 16943-16950.
38. Wang, Y.; Xie, T.; France-Lanord, A.; Berkley, A.; Johnson, J. A.; Shao-Horn, Y.; Grossman, J. C., Toward Designing Highly Conductive Polymer Electrolytes by Machine Learning Assisted Coarse-Grained Molecular Dynamics. *Chem. Mater.* **2020**, *32* (10), 4144-4151.
39. Attia, P. M.; Grover, A.; Jin, N.; Severson, K. A.; Markov, T. M.; Liao, Y.-H.; Chen, M. H.; Cheong, B.; Perkins, N.; Yang, Z., Closed-loop optimization of fast-charging protocols for batteries with machine learning. *Nature* **2020**, *578* (7795), 397-402.
40. Doan, H. A.; Agarwal, G.; Qian, H.; Counihan, M. J.; Rodríguez-López, J.; Moore, J. S.; Assary, R. S., Quantum Chemistry-Informed Active Learning to Accelerate the Design and Discovery of Sustainable Energy Storage Materials. *Chem. Mater.* **2020**.
41. Dave, A.; Mitchell, J.; Kandasamy, K.; Wang, H.; Burke, S.; Paria, B.; Póczos, B.; Whitacre, J.; Viswanathan, V., Autonomous Discovery of Battery Electrolytes with Robotic Experimentation and Machine Learning. *Cell Reports Physical Science* **2020**, 100264.
42. Jouny, M.; Luc, W.; Jiao, F., General techno-economic analysis of CO₂ electrolysis systems. *Industrial & Engineering Chemistry Research* **2018**, *57* (6), 2165-2177.
43. Bushuyev, O. S.; De Luna, P.; Dinh, C. T.; Tao, L.; Saur, G.; van de Lagemaat, J.; Kelley, S. O.; Sargent, E. H., What should we make with CO₂ and how can we make it? *Joule* **2018**, *2* (5), 825-832.
44. Lee, J.; Lee, W.; Ryu, K. H.; Park, J.; Lee, H.; Lee, J. H.; Park, K. T., Catholyte-free electroreduction of CO₂ for sustainable production of CO: concept, process development, techno-economic analysis, and CO₂ reduction assessment. *Green Chemistry* **2021**, *23* (6), 2397-2410.
45. Rumayor, M.; Dominguez-Ramos, A.; Perez, P.; Irabien, A., A techno-economic evaluation approach to the electrochemical reduction of CO₂ for formic acid manufacture. *Journal of CO₂ Utilization* **2019**, *34*, 490-499.
46. Somoza-Tornos, A.; Guerra, O. J.; Crow, A. M.; Smith, W. A.; Hodge, B.-M., Process modeling, techno-economic assessment, and life cycle assessment of the electrochemical reduction of CO₂: a review. *Iscience* **2021**, 102813.
47. Grim, R. G.; Huang, Z.; Guarneri, M. T.; Ferrell, J. R.; Tao, L.; Schaidle, J. A., Transforming the carbon economy: challenges and opportunities in the convergence of low-cost electricity and reductive CO₂ utilization. *Energy Environ. Sci.* **2020**, *13* (2), 472-494.
48. Ma, S.; Lan, Y.; Perez, G. M.; Moniri, S.; Kenis, P. J., Silver supported on titania as an active catalyst for electrochemical carbon dioxide reduction. *ChemSusChem* **2014**, *7* (3), 866-874.
49. Hoshi, N.; Kato, M.; Hori, Y., Electrochemical reduction of CO₂ on single crystal electrodes of silver Ag (111), Ag (100) and Ag (110). *J. Electroanal. Chem.* **1997**, *440* (1-2), 283-286.

50. Hori, Y.; Ito, H.; Okano, K.; Nagasu, K.; Sato, S., Silver-coated ion exchange membrane electrode applied to electrochemical reduction of carbon dioxide. *Electrochim. Acta* **2003**, *48* (18), 2651-2657.
51. Kim, C.; Jeon, H. S.; Eom, T.; Jee, M. S.; Kim, H.; Friend, C. M.; Min, B. K.; Hwang, Y. J., Achieving selective and efficient electrocatalytic activity for CO₂ reduction using immobilized silver nanoparticles. *Journal of the American Chemical Society* **2015**, *137* (43), 13844-13850.
52. Delacourt, C.; Ridgway, P. L.; Kerr, J. B.; Newman, J., Design of an electrochemical cell making syngas (CO+ H₂) from CO₂ and H₂O reduction at room temperature. *J. Electrochem. Soc.* **2007**, *155* (1), B42.
53. Jiang, K.; Kharel, P.; Peng, Y.; Gangishetty, M. K.; Lin, H.-Y. G.; Stavitski, E.; Attenkofer, K.; Wang, H., Silver nanoparticles with surface-bonded oxygen for highly selective CO₂ reduction. *ACS Sustainable Chemistry & Engineering* **2017**, *5* (10), 8529-8534.
54. Salvatore, D. A.; Weekes, D. M.; He, J.; Dettelbach, K. E.; Li, Y. C.; Mallouk, T. E.; Berlinguette, C. P., Electrolysis of Gaseous CO₂ to CO in a Flow Cell with a Bipolar Membrane. *ACS Energy Lett.* **2017**, *3* (1), 149-154.
55. Vermaas, D. A.; Smith, W. A., Synergistic electrochemical CO₂ reduction and water oxidation with a bipolar membrane. *ACS Energy Lett.* **2016**, *1* (6), 1143-1148.
56. Shiratsuchi, R.; Nogami, G., Pulsed electroreduction of CO₂ on silver electrodes. *J. Electrochem. Soc.* **1996**, *143* (2), 582.
57. Yano, H.; Shirai, F.; Nakayama, M.; Ogura, K., Electrochemical reduction of CO₂ at three-phase (gas| liquid| solid) and two-phase (liquid| solid) interfaces on Ag electrodes. *J. Electroanal. Chem.* **2002**, *533* (1-2), 113-118.
58. Kim, Y. E.; Kim, B.; Lee, W.; Ko, Y. N.; Youn, M. H.; Jeong, S. K.; Park, K. T.; Oh, J., Highly tunable syngas production by electrocatalytic reduction of CO₂ using Ag/TiO₂ catalysts. *Chem. Eng. J.* **2021**, *413*, 127448.
59. Lee, W. H.; Ko, Y.-J.; Choi, Y.; Lee, S. Y.; Choi, C. H.; Hwang, Y. J.; Min, B. K.; Strasser, P.; Oh, H.-S., Highly selective and scalable CO₂ to CO-Electrolysis using coral-nanostructured Ag catalysts in zero-gap configuration. *Nano Energy* **2020**, *76*, 105030.
60. Oh, S.; Park, Y. S.; Park, H.; Kim, H.; Jang, J. H.; Choi, I.; Kim, S.-K., Ag-deposited Ti gas diffusion electrode in proton exchange membrane CO₂ electrolyzer for CO production. *Journal of Industrial and Engineering Chemistry* **2020**, *82*, 374-382.
61. Sun, D.; Xu, X.; Qin, Y.; Jiang, S. P.; Shao, Z., Rational Design of Ag-Based Catalysts for the Electrochemical CO₂ Reduction to CO: A Review. *ChemSusChem* **2020**, *13* (1), 39-58.
62. Dinh, C.-T.; Burdyny, T.; Kibria, M. G.; Seifitokaldani, A.; Gabardo, C. M.; De Arquer, F. P. G.; Kiani, A.; Edwards, J. P.; De Luna, P.; Bushuyev, O. S., CO₂ electroreduction to ethylene via hydroxide-mediated copper catalysis at an abrupt interface. *Science* **2018**, *360* (6390), 783-787.
63. Kwon, Y.; Lum, Y.; Clark, E. L.; Ager, J. W.; Bell, A. T., CO₂ electroreduction with enhanced ethylene and ethanol selectivity by nanostructuring polycrystalline copper. *ChemElectroChem* **2016**, *3* (6), 1012-1019.
64. Yang, H. J.; Yang, H.; Hong, Y. H.; Zhang, P. Y.; Wang, T.; Chen, L. N.; Zhang, F. Y.; Wu, Q. H.; Tian, N.; Zhou, Z. Y., Promoting ethylene selectivity from CO₂ electroreduction on CuO supported onto CO₂ capture materials. *ChemSusChem* **2018**, *11* (5), 881-887.
65. Yang, P.-P.; Zhang, X.-L.; Gao, F.-Y.; Zheng, Y.-R.; Niu, Z.-Z.; Yu, X.; Liu, R.; Wu, Z.-Z.; Qin, S.; Chi, L.-P., Protecting copper oxidation state via intermediate confinement

for selective CO₂ electroreduction to C₂+ fuels. *Journal of the American Chemical Society* **2020**, *142* (13), 6400-6408.

66. Kibria, M. G.; Dinh, C. T.; Seifitokaldani, A.; De Luna, P.; Burdyny, T.; Quintero-Bermudez, R.; Ross, M. B.; Bushuyev, O. S.; García de Arquer, F. P.; Yang, P., A surface reconstruction route to high productivity and selectivity in CO₂ electroreduction toward C₂+ hydrocarbons. *Adv. Mater.* **2018**, *30* (49), 1804867.
67. Winiwarter, A.; Silvioli, L.; Scott, S. B.; Enemark-Rasmussen, K.; Sariç, M.; Trimarco, D. B.; Vesborg, P. C.; Moses, P. G.; Stephens, I. E.; Seger, B., Towards an atomistic understanding of electrocatalytic partial hydrocarbon oxidation: propene on palladium. *Energy Environ. Sci.* **2019**, *12* (3), 1055-1067.
68. Xie, J.; Zhang, Q.; Chuang, K. T., An IGC study of Pd/SDB catalysts for partial oxidation of propylene to acrylic acid. *J. Catal.* **2000**, *191* (1), 86-92.
69. Casebolt, R.; Levine, K.; Suntivich, J.; Hanrath, T., Pulse check: Potential opportunities in pulsed electrochemical CO₂ reduction. *Joule* **2021**.
70. Blanco, D. E.; Lee, B.; Modestino, M. A., Optimizing organic electrosynthesis through controlled voltage dosing and artificial intelligence. *Proceedings of the National Academy of Sciences* **2019**, *116* (36), 17683-17689.
71. Kim, C.; Bui, J. C.; Luo, X.; Cooper, J. K.; Kusoglu, A.; Weber, A. Z.; Bell, A. T., Tailored catalyst microenvironments for CO₂ electroreduction to multicarbon products on copper using bilayer ionomer coatings. *Nat. Energy* **2021**, *6* (11), 1026-1034.
72. Shiratsuchi, R.; Aikoh, Y.; Nogami, G., Pulsed electroreduction of CO₂ on copper electrodes. *J. Electrochem. Soc.* **1993**, *140* (12), 3479.
73. Nogami, G.; Itagaki, H.; Shiratsuchi, R., Pulsed Electroreduction of CO₂ on Copper Electrodes-II. *J. Electrochem. Soc.* **1994**, *141* (5), 1138.
74. Ishimaru, S.; Shiratsuchi, R.; Nogami, G., Pulsed Electroreduction of CO₂ on Cu-Ag Alloy Electrodes. *J. Electrochem. Soc.* **2000**, *147* (5), 1864.
75. Yano, J.; Morita, T.; Shimano, K.; Nagami, Y.; Yamasaki, S., Selective ethylene formation by pulse-mode electrochemical reduction of carbon dioxide using copper and copper-oxide electrodes. *J. Solid State Electrochem.* **2007**, *11* (4), 554-557.
76. Kumar, B.; Brian, J. P.; Atla, V.; Kumari, S.; Bertram, K. A.; White, R. T.; Spurgeon, J. M., Controlling the product syngas H₂: CO ratio through pulsed-bias electrochemical reduction of CO₂ on copper. *ACS Catalysis* **2016**, *6* (7), 4739-4745.
77. Jännsch, Y.; Leung, J. J.; Hämmerle, M.; Magori, E.; Wiesner-Fleischer, K.; Simon, E.; Fleischer, M.; Moos, R., Pulsed potential electrochemical CO₂ reduction for enhanced stability and catalyst reactivation of copper electrodes. *Electrochem. Commun.* **2020**, *121*, 106861.
78. Arán-Ais, R. M.; Scholten, F.; Kunze, S.; Rizo, R.; Cuenya, B. R., The role of in situ generated morphological motifs and Cu (I) species in C₂+ product selectivity during CO₂ pulsed electroreduction. *Nat. Energy* **2020**, *5* (4), 317-325.
79. Engelbrecht, A.; Uhlig, C.; Stark, O.; Hämmerle, M.; Schmid, G.; Magori, E.; Wiesner-Fleischer, K.; Fleischer, M.; Moos, R., On the electrochemical CO₂ reduction at copper sheet electrodes with enhanced long-term stability by pulsed electrolysis. *J. Electrochem. Soc.* **2018**, *165* (15), J3059.
80. Strain, J. M.; Gulati, S.; Pishgar, S.; Spurgeon, J. M., Pulsed Electrochemical Carbon Monoxide Reduction on Oxide-Derived Copper Catalyst. *ChemSusChem* **2020**, *13* (11), 3028-3033.

81. Casebolt, R.; Kimura, K. W.; Levine, K.; Cimada DaSilva, J. A.; Kim, J.; Dunbar, T. A.; Suntivich, J.; Hanrath, T., Effect of electrolyte composition and concentration on pulsed potential electrochemical CO₂ reduction. *ChemElectroChem* **2021**, *8* (4), 681-688.
82. Kimura, K. W.; Casebolt, R.; Cimada DaSilva, J.; Kauffman, E.; Kim, J.; Dunbar, T. A.; Pollock, C. J.; Suntivich, J.; Hanrath, T., Selective electrochemical CO₂ reduction during pulsed potential stems from dynamic interface. *ACS Catalysis* **2020**, *10* (15), 8632-8639.
83. Kimura, K. W.; Fritz, K. E.; Kim, J.; Suntivich, J.; Abruña, H. D.; Hanrath, T., Controlled Selectivity of CO₂ Reduction on Copper by Pulsing the Electrochemical Potential. *ChemSusChem* **2018**, *11* (11), 1781-1786.
84. Xu, Y.; Edwards, J. P.; Liu, S.; Miao, R. K.; Huang, J. E.; Gabardo, C. M.; O'Brien, C. P.; Li, J.; Sargent, E. H.; Sinton, D., Self-cleaning CO₂ reduction systems: unsteady electrochemical forcing enables stability. *ACS Energy Lett.* **2021**, *6* (2), 809-815.